Journal of Biomedical Optics

SPIEDigitalLibrary.org/jbo

Calibration-free structured-illumination photoacoustic flowgraphy of transverse flow in scattering media

Junjie Yao
Rebecca C. Gilson
Konstantin I. Maslov
Lidai Wang
Lihong V. Wang

Calibration-free structured-illumination photoacoustic flowgraphy of transverse flow in scattering media

Junjie Yao, Rebecca C. Gilson, Konstantin I. Maslov, Lidai Wang, and Lihong V. Wang*
Washington University in St. Louis, Department of Biomedical Engineering, Optical Imaging Laboratory, St. Louis, Missouri 63130

Abstract. We propose a calibration-free photoacoustic (PA) method for transverse flow measurements. In this method, a pulsed periodically structured (i.e., grating patterned) optical beam is used to illuminate flowing absorptive particles in an optically scattering medium. The PA signal amplitudes measured over consecutive laser pulses carry an imprint of the illumination structure. The modulation frequency of the imprint is proportional to the component of the flow speed projected onto the normal axis of the striped illumination pattern. This method can tolerate high particle density, and is insensitive to the particle size, thus calibration-free. Bovine blood and microsphere phantoms were used to validate the proposed method. Blood flow in a mouse ear was measured *in vivo* as well. [DOI: 10.1117/1.JBO.19.4.046007]

Keywords: photoacoustic flowgraphy; structured illumination; frequency shift; particle size independent.

Paper 130871R received Dec. 5, 2013; revised manuscript received Feb. 27, 2014; accepted for publication Mar. 21, 2014; published online Apr. 9, 2014.

1 Introduction

The ability to measure blood flow is important in the diagnosis and treatment of many diseases, such as burns, port-wine stains, and cancers.[1] Blood flow measurement by photoacoustic (PA) imaging is gaining interest, as it takes advantage of weak acoustic scattering and high optical absorption contrast.[2–7] Compared with ultrasound Doppler imaging, PA flow measurement has superior detection sensitivity. Depending on acoustic scattering, Doppler ultrasound suffers from a lack of sensitivity to red blood cells (RBCs), especially in measuring slow blood flow (<1 mm/s). Slowly flowing RBCs yield small Doppler shifts that are easily obscured by the motion of the surrounding tissue. In comparison, PA flow measurement, based on optical absorption contrast, can quantify slow flow speed accurately by sensing optical absorption by blood. Optical-resolution photoacoustic microscopy (OR-PAM), a major implementation of PA imaging, focuses on capillary level spatial resolution within the optical diffusion limit (~1 mm in tissue).[8,9] OR-PAM has been used to measure transverse blood flow speed based on bandwidth broadening, while the flow direction can be determined using bidirectional scanning.[6] A phantom calibration is needed to account for the particle size because the transit time of a RBC traveling across the optical focus determines the bandwidth broadening. Moreover, tissue scattering reduces the optical focusing capability. The enlarged focal spot in deeper tissue results in an underestimation of flow speeds. However, for *in vivo* applications where absolute flow speeds are of interest, accurate tissue-specific or particle-specific calibrations are not always available, since the tissue environment is complex and the intrinsic particles (most commonly, RBCs) come in different sizes, orientations, and concentrations.

2 Methods

Here, we propose to measure transverse blood flow by using structured light illumination, where a one-dimensional (1-D) optical fringe pattern is formed with its normal axis coplanar with the flow direction.[10] Here, the normal axis (x axis) is defined as the direction perpendicular to the fringes. As absorptive particles flow across the lighted and shaded portions of the fringes, they are illuminated and shadowed, respectively, which modulate the PA signals acquired over consecutive laser pulses, as shown in Fig. 1(a). The total PA signals can be modeled by integrating the PA signals from all particles within the acoustic detection volume.

First, the 1-D excitation profile is modeled as

$$M(x) \propto 1 + a\cos\left(2\pi\frac{x}{d}\right), \tag{1}$$

where a is the modulation depth of the illumination pattern, d is the fringe pitch. For simplicity, the initial phase in the modulation term is set to zero by shifting the x axis.

The acoustic detection sensitivity profile is approximated with a Gaussian function as

$$B(x) \propto \exp\left(-\frac{x^2}{2L^2}\right), \tag{2}$$

where L is the standard deviation of the profile. The full width at half maximum (FWHM) of the profile is $D = 2\sqrt{2\ln 2}L$.

Here, we define the flight time axis of each time-resolved PA signal as the "fast time" axis, and the laser pulse sampling axis over consecutive laser firings as the "slow time" axis.[2,6] If the particles maintain the same distribution as they flow across the detection zone, the PA signal along the slow time axis can be expressed as

$$p(t_s) \propto \int_{-\infty}^{\infty} M(x)B(x)f(x - v_x t_s)\mathrm{d}x, \tag{3}$$

where p is the PA signal amplitude, t_s is the slow time across consecutive laser pulses, $f(x)$ denotes the particle density

*Address all correspondence to: Lihong V. Wang, E-mail: lhwang@wustl.edu

0091-3286/2014/$25.00

distribution along the x axis observed at $t_s = 0$, and v_x is the particle flow velocity projected onto the x axis.

Because $M(x)$ and $B(x)$ are both even functions, Eq. (3) can be rewritten as

$$p(t_s) \propto \int_{-\infty}^{\infty} M(x)B(x)f(-v_x t_s - x)\mathrm{d}x. \tag{4}$$

Here, we define the following function

$$g(x) = (MB * f)(x), \tag{5}$$

where * denotes convolution. Then we have

$$p(t_s) \propto g(-v_x t_s). \tag{6}$$

Taking the Fourier transformation of $g(x)$ gives

$$\tilde{G}(k_x) = [\tilde{M}(k_x) * \tilde{B}(k_x)]\tilde{F}(k_x), \tag{7}$$

where $\tilde{G}(k_x)$, $\tilde{B}(k_x)$, $\tilde{M}(k_x)$, and $\tilde{F}(k_x)$ are the Fourier transforms of $g(x)$, $B(x)$, $M(x)$ and $f(x)$, respectively.

We have

$$\tilde{B}(k_x) \propto \exp\left(-\frac{L^2 k_x^2}{2}\right), \tag{8}$$

$$\tilde{M}(k_x) \propto \delta(k_x) + \frac{a}{2}\delta\left(k_x \pm \frac{2\pi}{d}\right). \tag{9}$$

If the particle density $f(x)$ is a temporally ergodic random process following a normal distribution with a nonzero mean, $\tilde{F}(k_x)$ can be written as

$$\tilde{F}(k_x) \propto \delta(k_x) + b\tilde{F}_{\mathrm{AC}}(k_x), \tag{10}$$

where $\tilde{F}_{\mathrm{AC}}(k_x)$ is the Fourier transform of the AC (zero-mean) component of $f(x)$. Here, an ergodic process refers to a random process whose statistical properties, such as the mean and variance of the process, can be deduced from a sufficiently long sample of the process. In our case, it means that the random distribution of particle density can be fully characterized from a set of consecutive measurements.

$\tilde{F}_{\mathrm{AC}}(k_x)$ has a flat spectrum if $f(x)$ has a zero correlation length. b denotes the relative magnitude of $\tilde{F}_{\mathrm{AC}}(k_x)$. If the particles can be approximated as microspheres, b can be estimated as[11,12]

$$b \approx \frac{2J_1(\pi s/d)}{\sqrt{N}(\pi s/d)}, \tag{11}$$

where J_1 is the first-order Bessel function of the first kind, s is the particle diameter, and N is the number of particles within the detection region.

Substituting Eqs. (8)–(10) into Eq. (7) leads to

$$\tilde{G}(k_x) \propto \left[\delta(k_x) + \frac{ab}{2}\delta\left(k_x \pm \frac{2\pi}{d}\right)\right] * \exp\left(-\frac{L^2 k_x^2}{2}\right). \tag{12}$$

Combining Eqs. (6) and (12) and using the scaling property of the Fourier transformation, we get

$$\tilde{P}(\omega) \propto \tilde{G}\left(-\frac{\omega}{v_x}\right) \propto \left[\delta(\omega) + \frac{ab}{2}\delta\left(\omega \pm 2\pi\frac{v_x}{d}\right)\right] * \exp\left(-\frac{L^2\omega^2}{2v_x^2}\right), \tag{13}$$

where $\tilde{P}(\omega)$ is the Fourier transform of $p(t_s)$.

Clearly, Eq. (13) shows that $\tilde{P}(\omega)$ has three peaks at 0 and $\pm 2\pi v_x/d$, each with an FWHM of $2\sqrt{2\ \ln\ 2}v_x/L$. We can compute the flow speed through the peak frequency of the sidebands ω_p, as $v_x = \omega_p d/(2\pi)$ or simply $v_x = d/T_p$, where T_p is the period of the sidebands. The FWHM of the peaks can also be used to quantify the flow speed.

Equation (13) shows that the peak frequency ω_p depends on the flow velocity and the fringe pitch period but does not change with the particle size. In essence, it is the particle transit time over one fringe pitch that determines the peak frequency. In our method, the transit time is defined as the time during which the center of the particle (or any other positions) passes through the centers of two consecutive strips (or any other corresponding positions). This particle size insensitivity originates from the periodically patterned illumination. As a particle (e.g., a RBC) passes through the illumination fringe, the transit time is related only to the fringe pitch and the particle speed. In other words, when we calculate the transit time, the particle can be treated as an infinitely small "absorption center", regardless of the actual particle size. A mixture of particles with various sizes will not impact the measurement. This is different from the case in which only a single illumination point or strip is present,[4–6] where the transit time depends on the illumination spot size, the particle speed, and the particle size. Within the optical diffusion limit, although tissue scattering of light may reduce the modulation depth and blur the fringe pattern, the pitch period is maintained. Furthermore, the acoustic detection sensitivity and the distribution of the laser intensity across the fringe pattern only affect the spectral bandwidth, not its peak frequency.

The amplitude at the frequency peak ω_p depends on the modulation depth of the excitation pattern and the amplitude of $\tilde{F}_{\mathrm{AC}}(k_x)$. $\tilde{F}_{\mathrm{AC}}(k_x)$ spreads approximately evenly over its bandwidth of about $2\pi/s$, where s is the particle size. Correspondingly, for $\tilde{P}(\omega)$ to have a significant amplitude at $\omega_p = 2\pi v_x/d$, the fringe pitch d should be larger than the particle size s.

Although the particle size does not directly impact the flow speed measurement, it will affect the flow measurement accuracy. We know that a finite particle size is one of the major sources for the direct current (DC) and low-frequency signal components measured over consecutive laser pulses. Our method eventually becomes less accurate when the particle size increases. The overall signal-to-noise ratio (SNR) is closely related to the modulation depth, because signal fluctuations due to laser intensity instability are proportional to the DC signal component. Here, SNR is defined as the ratio between the alternative current (AC) component of the signal and the standard deviation of signal fluctuations induced by thermal noise and laser pulse instability. To ensure a decent modulation depth (>0.5), the particle diameter should not exceed half of the fringe pitch.

The amplitude of $\tilde{F}_{\mathrm{AC}}(k_x)$ is roughly proportional to the square root of the average particle concentration, which enables flow measurement with high particle density. However, the PA signal variation due to laser fluctuations is proportional to the

average particle concentration (i.e., the DC component). Since b decreases with increasing average particle concentration, the contribution from laser fluctuations will eventually overwhelm the contribution from $\tilde{F}_{AC}(k_x)$. While laser fluctuations can be partially compensated by a photodiode reading, it is principally the noise level that limits the maximum applicable particle concentration in this method. When the circulating system contains only homogeneous absorbers, such as ink solution, we can treat the particle density as infinitely high. An infinitely high particle concentration leads to a modulation depth of zero, and thus our method does not work for homogeneous flow. Fortunately, in biological systems, the most common flow is blood flow, where the RBCs are particles with a volumetric density of ~45%. If the particle density in the detection volume is inhomogeneous and as long as the particles have the same flow speed, they will contribute to the same frequency. Due to their lower SNR, it is possible that the high-density regions contribute less than the low-density regions if they happen to have different flow speeds. In our theoretical model, we assume that the particle density is statistically uniform within the detection volume. This assumption is generally valid since our detection region is relatively small and RBCs in blood are approximately uniform in the statistical sense.

3 Results

3.1 *Experimental Setup*

The experimental setup is shown in Fig. 1(b), which is adapted from a previously published double-illumination photoacoustic microscopy (PAM) system.[13] A tunable dye laser (CBR-D, Sirah Inc., Grevenbroich, Germany) pumped by a Nd:YLF laser (INNOSAB, Edgewave Inc., Würselen, Germany) irradiates the sample with a repetition rate of 4 kHz and a pulse energy of ~200 nJ. An iris selects only the center part of the beam with relatively uniform light intensity. The 2.0-mm-diameter laser beam is directed onto a Ronchi-ruling (NT57-903, Edmunds Optics Inc., Barrington, 5 line pairs per mm), and a tube lens (focal length 160 mm) refocuses the subsequent diffraction orders of −1, 0, and 1, into the back focal plane of an objective lens (numerical aperture 0.4). The beam is recollimated by the objective lens and intersects at the focal plane, where interference generates an intensity pattern with a demagnified fringe pitch of 12.5 μm, an

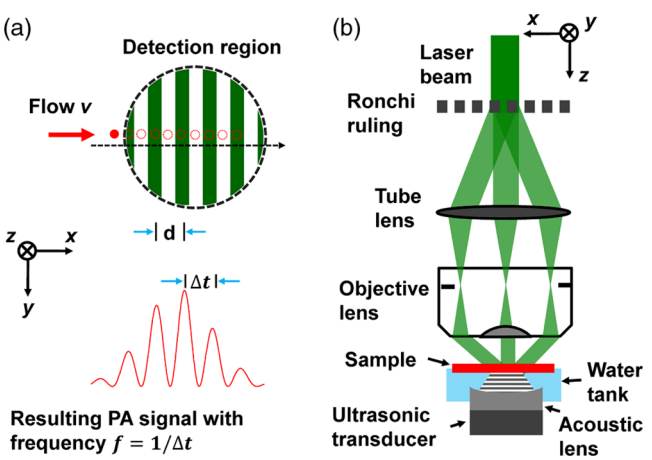

Fig. 1 Fringe-based photoacoustic flowgraphy. (a) Illustration of the flow measurement principle. (b) Schematic of the experimental system.

averaged fringe contrast of 0.46, and a total illumination radius of ~60 μm, measured by a beam profiler [Fig. 2(a)]. The laser intensity heterogeneity within the acoustic detection region is less than 2% and thus negligible [Fig. 2(b)]. Note that the Ronchi-ruling pattern is not a strictly sinusoidal function but a square function with a duty cycle of 50%. However, because of the low-pass filtering of the imaging system, the harmonics of the fundamental frequency are largely suppressed. Fourier transformation of the actual laser intensity on the sample surface shows that the harmonics are at least 20 times weaker than the fundamental frequency component and thus negligible. Therefore, the sinusoidal approximation of the illumination pattern in Eq. (1) is valid.

The resultant acoustic waves are then detected with a focused ultrasonic transducer (V214-BC, Olympus NDT, Inc., Waltham), placed confocally with the optical objective. To check the size of the fringe pattern, a 6-μm-diameter carbon fiber was aligned perpendicular to the normal axis and scanned along the normal axis. The carbon fiber served as an absorber to create the PA detection profile. The period of the PA signal amplitude further confirmed the fringe pitch of 12.5 μm [solid line in Fig. 2(c)]. The FWHM of the Gaussian-shape signal envelope was ~71 μm [dashed line in Fig. 2(c)], determined by the distribution of acoustic detection sensitivity. The measured FWHM indicates that L in Eq. (2) equals to 30.2 μm.

3.2 *Flow Measurement on Bovine Blood Phantom*

A syringe pump (BSP-99M, Braintree Scientific Inc., Braintree) was used to control the speed of defibrinated bovine blood

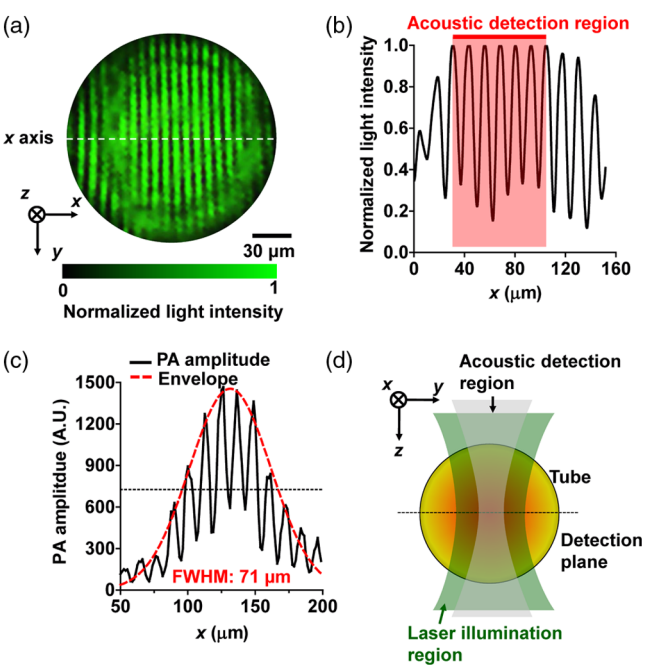

Fig. 2 Characterization of the fringe-based photoacoustic flowgraphy. (a) Illumination fringe pattern captured by a CCD camera, showing a fringe pitch of 12.5 μm. The x axis is defined as the line perpendicular to the fringes. (b) The laser intensity profile along the centerline of the illumination pattern, showing a peak intensity variation of <2% in the acoustic detection region. (c) PA signal amplitude measured from a 6-μm-carbon fiber moving across the fringe pattern. Red dashed line: Gaussian fit of the signal envelope. (d) Illustration of the illumination and detection regions over the flowing sample.

(hematocrit 45%) flowing in a plastic tube (inner diameter 300 μm). The tube was fixed in a water tank and the flow direction was adjusted to be aligned with the normal axis, as shown in Fig. 1(f). The bottom of the water tank was sealed with a piece of optically and acoustically transparent membrane. The PA signal at a wavelength of 570 nm was recorded for 4000 laser pulses. The PA signal at the center plane of the tube was extracted and formed a new data vector, and the DC component of the vector was removed by subtracting its mean value. Then, the vector was passed through a fast Fourier transformation, where the amplitude spectral density was calculated. The above measurement was repeated 200 times, and the mean amplitude spectral density was used to compute the flow speed. By controlling the speed of the syringe pump, the blood flow speed at the tube center was adjusted from 0 to 9.0 mm/s. Figures 3(a)–3(c) show the normalized amplitude spectral densities at three representative flow speeds of 1.2, 2.4, and 4.8 mm/s. The average flow speed can be estimated based on the peak frequency. As shown in Fig. 3(d), the measured peak frequency is proportional to the preset flow speed, agreeing well with the theoretical model. The measurement error is estimated to be within 0.05 mm/s, based on the root mean square of the errors. From the results shown in Figs. 3(a)–3(c), we can also see the frequency spectrum broadens as the flow speed increases. As predicted by Eq. (13), the nonuniform acoustic detection profile results in a −3 dB broadening of ~20%.

The sampling region in Fig. 3 is determined by the acoustic detection region, which can be approximated as a disk with a diameter of 70 μm and a thickness of 15 μm [as shown in Fig. 2(d)]. We notice that within each detection region, the flow speed itself is nonuniform. Considering the acoustic detection profile, this flow speed variation would also result in a 5% peak broadening toward the lower frequency side. This broadening is negligible since it is smaller than the broadening induced by the nonuniform acoustic detection profile. Due to the acoustic detection profile, the flow speed in the center of the detection region contributes most to the final spectrum. Therefore, in Figs. 3(a)–3(c), the measured peak frequencies should mostly represent the flow speeds at the center of the detection region.

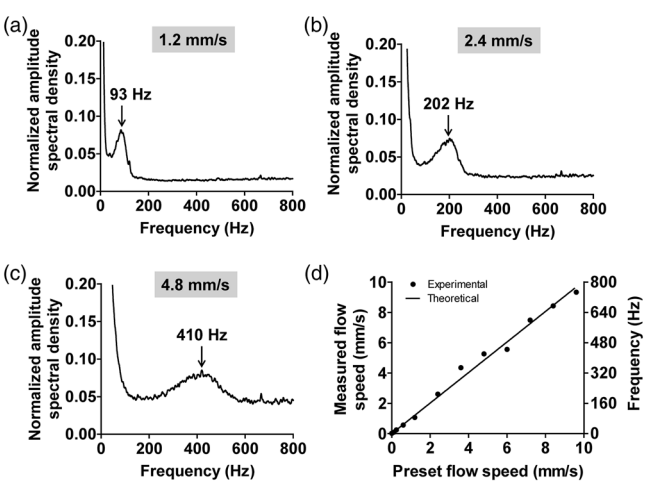

Fig. 3 Fringe-based PA flowgraphy of whole bovine blood phantom. (a–c) show the normalized amplitude spectral densities for three representative flow speeds. (d) Measured flow speed and peak modulation frequency as a function of the preset speed. The solid line is the theoretical calculation.

3.3 *Flow Measurement on Microspheres with Different Sizes*

The influence of particle size on the flow measurement was studied with three types of particles: red microspheres with diameters of 3 and 6 μm, and black microspheres with a diameter of 10 μm (Polysciences, Inc., Warrington). The three flow samples were suspensions of these microspheres in distilled water with a concentration of $\sim 4.5 \times 10^7$ particles/mL. Sodium polytungstate was added to match the mass density, and approximately 10% volume of Tween-20 oil (Sigma-Aldrich Inc., St. Louis) was added to reduce microsphere aggregation. The results in Fig. 4(a) show that the particle size did not affect the measured peak frequencies, which agrees with our theoretical model.

3.4 *Measurement of Axial Flow Speed Profile*

Taking advantage of OR-PAM's high axial resolution of 15 μm,[8] we measured the flow speed profile along the radial direction of the tube with three different flow speeds. The diameter of the microspheres was 6 μm, and the tube diameter was 300 μm. As shown in Fig. 4(b), the following expected parabolic distribution fits all three profiles well:

$$v_x(z) = v_{x-\max}\left[1 - \left(\frac{z - z_0}{R}\right)^2\right]. \tag{14}$$

Here, z is the axial coordinate in the depth direction, z_0 is the tube center, R is the tube radius, and $v_{x-\max}$ is the flow speed at the tube center. z_0 and R can be measured directly from the PA images, and $v_{x-\max}$ is the unknown parameter determined by fitting the data. Note that the measured flow speeds close to the bottom of the tube [arrows in Fig. 4(b)] are less accurate because of weak signal strength due to the limited light penetration. Strictly speaking, the measured flow speed at each depth should be the average speed within the detection plane. As we discussed above, since the tube diameter is much larger than the FWHM of the detection region, the actual peak velocity at the tube centerline contributes most to the final spectrum. As the detection plane moves closer to the boundaries of the tube, the speed variation within the plane decreases. Overall, Eq. (14) is still a valid approximation for the flow speed profile along the depth.

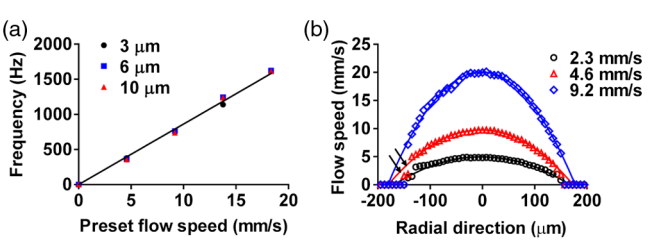

Fig. 4 Fringe-based PA flowgraphy of microspheres with different diameters. (a) Peak frequency of the PA signal as a function of flow speed with different particle diameters. Solid line: theoretical calculation. (b) Flow speed distribution of 6-μm-diameter particles with different average flow speeds along the radial direction of a cylindrical tube. Solid lines denote parabolic fittings.

3.5 *In Vivo Flow Measurement on a Mouse Ear*

An *in vivo* experiment was performed on the ear of a female ND4 Swiss Webster mouse (Harlan Laboratory Inc., Indianapolis). The animal experiment was performed in accordance with protocols approved by the Animal Studies Committee of Washington University in St. Louis, Missouri. The dorsal side of the ear was imaged with the animal lying on its back. A 1×1 mm^2 region was first imaged at 570 nm using the traditional reflection-mode OR-PAM [Fig. 5(a)].[8] A vein with a diameter of 71 μm was chosen for flow measurement at its center. Figure 5(b) shows the frequency spectral density under normal conditions, where the peak frequency at 150 Hz corresponded to a mean blood flow speed of ~1.9 mm/s, which agrees with the literature.[14] As a simple test to confirm the source of the measured signal, pressure was applied at the root of the ear to cuff the blood flow in the vein, and the flow speed was measured again. No frequency peak was observed under this condition, confirming that the blood flow had stopped.

4 Discussion

Currently, with the illumination fringe pitch of 12.5 μm, the maximum measurable flow speed is ~25 mm/s, as determined by the laser repetition rate of 4 kHz. The maximum measurable speed can be improved by using a faster repetition laser system. However, the ultimate limitation on the maximum measurable flow speed is the noise level. When the flow speed increases, the power spectrum broadens while the spectral amplitude decreases and eventually approaches the noise level. Increasing the laser power or improving the transducer sensitivity can extend the ultimate maximum measurable flow speed. The minimum measureable flow speed is ~0.01 mm/s, which represents the velocity sensitivity of the system, and it is determined by the total sampling time of 1 s or a frequency resolution of 1 Hz. Increasing the number of samples can reduce the minimum further. The ultimate limit of the velocity sensitivity can be estimated from the spectral broadening due to the Brownian motion of particles.

In the above phantom experiments, a temporal resolution of 1 s was achieved. Time-varying blood flows with a frequency greater than 1 Hz would be temporally averaged in our method. Of course, shortening the sampling time will improve the temporal resolution at the expense of SNR. For the measurement zone, we can actually penetrate about 200 μm into the blood tube (Fig. 3) and 300 μm into the microsphere tube (Fig. 4).

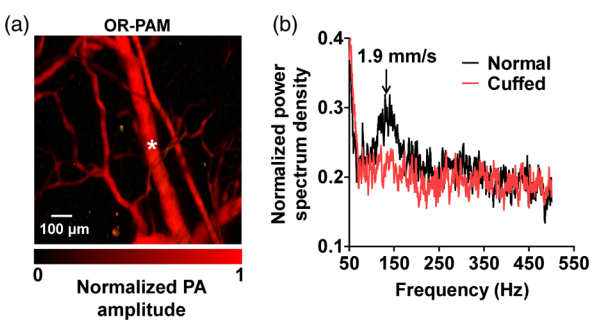

Fig. 5 Fringe-based PA blood flowgraphy in a mouse ear. (a) Photoacoustic microscopy of the mouse ear vasculature, where the blood flow at the center of a vein was measured, as marked by the star. (b) Frequency spectral densities measured before and after the vein was cuffed.

This measurement zone is largely limited by light attenuation, although the depth resolution of 15 μm is provided by the acoustic bandwidth. For example, the blood absorption coefficient is about 240 cm^{-1} at 570 nm wavelength unless another optical wavelength is chosen for deeper penetration. Based on the signal strength at the tube surface, the estimated noise equivalent penetration depth in blood is ~200 μm. By carefully adjusting the laser exposure within the American National Standards Institute (ANSI) limit, we can penetrate at least half the diameter of the blood tube.

The current method is not sensitive to the flow direction. One possible solution is to use bidirectional scanning of the fringes, as in our previous report.[6] In practice, if the blood flow is not parallel to the fringe normal, only the projected flow component contributes to the modulation frequency. However, the total blood flow speed can then be determined by simple trigonometry unless the flow is perpendicular to the fringe normal. Another option is to rotate the fringes and take multiple measurements. The depth range, in which a clear illumination pattern can be formed, is determined by the focal zone of the objective and the scattering in the tissue. For the light penetration depth in tissue, due to tissue scattering, a clear illumination pattern can be maintained up to approximately one transport mean free path (~1 mm in soft tissue). Within the optical diffusion limit, this method can be potentially used to study blood flow in skin cancers, and gastrointestinal cancers when implemented with endoscopic PAM.[15,16] Selecting longer wavelengths in the near infrared (NIR) regime can improve the penetration depth in tissue due to decreased blood absorption. Because the ANSI limit in the NIR region (100 mJ/cm^2) is five times higher than that in the visible region, the decreased signal strength due to lower blood absorption in the NIR region can be partially compensated by increasing the illumination fluence.[9]

5 Conclusion

In summary, we have developed a photoacoustic flow measurement method based on spatially structured illumination. This method does not need calibration and can measure blood flow over a wide range of speeds with good sensitivity. In addition, it can be used with varied particle sizes and high particle density. In conjunction with dual wavelength excitation and bidirectional scanning, this method can be potentially used for measuring the metabolic rate of oxygen.[17]

Acknowledgments

The authors would like to thank Professor James Ballard for manuscript editing. We also appreciate technical assistance and useful discussions with Arie Krumholz, Yong Zhou Liang S. Gao, and Yan Liu. This research was supported by the National Institutes of Health (Grant Nos. DP1 EB016986 (NIH Director's Pioneer Award), R01 EB016963, R01 EB008085, R01 CA134539, U54 CA136398, R01 CA157277, and R01 CA159959. L.V.W. has a financial interest in Microphotoacoustics, Inc. and Endra, Inc., which, however, did not support this work.

References

1. P. Vaupel, F. Kallinowski, and P. Okunieff, "Blood-flow, oxygen and nutrient supply, and metabolic microenvironment of human-tumors: a review," *Cancer Res.* **49**(23), 6449–6465 (1989).

2. J. Yao and L. V. Wang, "Transverse flow imaging based on photoacoustic Doppler bandwidth broadening," *J. Biomed. Opt.* **15**(2), 021304 (2010).
3. H. Fang, K. Maslov, and L. V. Wang, "Photoacoustic Doppler effect from flowing small light-absorbing particles," *Phys. Rev. Lett.* **99**(18), 184501 (2007).
4. H. Fang and L. H. V. Wang, "M-mode photoacoustic particle flow imaging," *Opt. Lett.* **34**(5), 671–673 (2009).
5. A. Sheinfeld and A. Eyal, "Photoacoustic thermal diffusion flowmetry," *Biomed. Opt. Express* **3**(4), 800–813 (2012).
6. J. Yao et al., "In vivo photoacoustic imaging of transverse blood flow by using Doppler broadening of bandwidth," *Opt. Lett.* **35**(9), 1419–1221 (2010).
7. J. Brunker and P. Beard, "Pulsed photoacoustic Doppler flowmetry using time-domain cross-correlation: accuracy, resolution and scalability," *J. Acous. Soc. Am.* **132**(3), 1780–1791 (2012).
8. K. Maslov et al., "Optical-resolution photoacoustic microscopy for in vivo imaging of single capillaries," *Opt. Lett.* **33**(9), 929–931 (2008).
9. J. Yao and L. V. Wang, "Photoacoustic microscopy," *Laser Photo. Rev.* **7**(5), 758–778 (2013).
10. M. Funatsu et al., "Study on light scattering velocimetry by using Ronchi-rulings," *Marine Eng.* **44**(1), 157–164 (2009).
11. W. M. Farmer, "Measurement of particle-size, number density, and velocity using a laser interferometer," *Appl. Opt.* **11**(11), 2603–2612 (1972).
12. W. M. Farmer and D. B. Brayton, "Analysis of atmospheric laser Doppler velocimeters," *Appl. Opt.* **10**(10), 2319–2324 (1971).
13. J. Yao et al., "Double-illumination photoacoustic microscopy," *Opt. Lett.* **37**(4), 659–661 (2012).
14. J. H. Barker et al., "The hairless mouse ear for in vivo studies of skin microcirculation," *Plast Reconstr. Surg.* **83**(6), 948–959 (1989).
15. J. M. Yang et al., "Simultaneous functional photoacoustic and ultrasonic endoscopy of internal organs in vivo," *Nat. Med.* **18**(8), 1297–1303 (2012).
16. J.-M. Yang et al., "A 2.5-mm diameter probe for photoacoustic and ultrasonic endoscopy," *Opt. Express*, **20**(21), 23944–23953 (2012).
17. J. Yao et al., "Label-free oxygen-metabolic photoacoustic microscopy in vivo," *J. Biomed. Opt.* **16**(7), 076003 (2011).

Junjie Yao is currently a postdoctoral research associate at Washington University in St. Louis, Missouri.

Rebecca C. Gilson is currently a graduate student at Washington University in St. Louis, Missouri.

Konstantin I. Maslov is currently a research associate professor at Washington University, in St. Louis, Missouri.

Lidai Wang is currently a postdoctoral research associate at Washington University, in St. Louis, Missouri.

Lihong V. Wang holds the Beare distinguished professorship at Washington University, in St. Louis, Missouri.